catalysts

MDPI

Article

Heterojunction Design between WSe_2 Nanosheets and TiO_2 for Efficient Photocatalytic Hydrogen Generation

Xu Guo [1,*], Xing Liu [1], Jing Shan [1], Guangtao Zhao [1] and Shengzhong (Frank) Liu [1,2,3,*]

[1] Shaanxi Key Laboratory for Advanced Energy Devices, Shaanxi Engineering Lab for Advanced Energy Technology, School of Materials Science and Engineering, Shaanxi Normal University, Xi'an 710119, China
[2] Center of Materials Science and Optoelectronics Engineering, University of Chinese Academy of Sciences, Beijing 100049, China
[3] Dalian Institute of Chemical Physics, Chinese Academy of Sciences, Dalian 116023, China
* Correspondence: guoxu@snnu.edu.cn (X.G.); szliu@dicp.ac.cn (S.L.)

Abstract: Design and fabrication of efficient and stable photocatalysts are critically required for practical applications of solar water splitting. Herein, a series of WSe_2/TiO_2 nanocomposites were constructed through a facile mechanical grinding method, and all of the nanocomposites exhibited boosted photocatalytic hydrogen evolution. It was discovered that the enhanced photocatalytic performance was attributed to the efficient electron transfer from TiO_2 to WSe_2 and the abundant active sites provided by WSe_2 nanosheets. Moreover, the intimate heterojunction between WSe_2 nanosheets and TiO_2 favors the interfacial charge separation. As a result, a highest hydrogen evolution rate of 2.28 mmol/g·h, 114 times higher than pristine TiO_2, was obtained when the weight ratio of $WSe_2/(WSe_2 + TiO_2)$ was adjusted to be 20%. The designed WSe_2/TiO_2 heterojunctions can be regarded as a promising photocatalysts for high-throughput hydrogen production.

Keywords: photocatalysts; WSe_2 nanosheets; TiO_2; nanocomposites; hydrogen

Citation: Guo, X.; Liu, X.; Shan, J.; Zhao, G.; Liu, S. Heterojunction Design between WSe_2 Nanosheets and TiO_2 for Efficient Photocatalytic Hydrogen Generation. *Catalysts* **2022**, *12*, 1668. https://doi.org/10.3390/catal12121668

Academic Editors: Xiangjiu Guan and Shichao Zong

Received: 28 November 2022
Accepted: 16 December 2022
Published: 19 December 2022

1. Introduction

Green and sustainable energy is urgently required for the rapid development of human beings. Hydrogen, as a type of green and renewable energy carrier, is considered to be an ideal substitute for fossil fuels in the future [1–3]. Solar energy conversion to hydrogen via photocatalysts holds great promise for hydrogen generation owing to the advantages of being environmentally friendly and high product purity [4–6]. Numerous semiconductors, including metal oxides, sulfides, phosphides, and polymers, are applied to photocatalytic hydrogen generation, and impressive achievements have been made in the past decades [7–10]. TiO_2, as a prototype photocatalyst, has been widely studied for solar water splitting owing to its chemical stability, nontoxicity, and low cost [11–15]. For example, (001)-facet-exposed ultrathin anatase TiO_2 nanosheets was designed for hydrogen generation [16]. However, single TiO_2 exhibits poor photocatalytic efficiency owing to its inability to absorb visible light, fast charge carrier recombination, and a slow interfacial hydrogen-production reaction [17–19]. Many approaches, such as doping, sensitizing, and surface hydrogeneration, are devoted to improving the photocatalytic performance and loading cocatalysts has been demonstrated as an effective way to boost the photocatalytic activity of TiO_2 [20–22].

Noble metals such as Pt, Au, Pd, etc. are widely applied as cocatalysts to improve the photocatalytic efficiency of TiO_2 owing to their low overpotentials and superior conductivity [23–25]. For example, Pt decorated anatase-TiO_2/H-rutile TiO_2 heterophase homojunctions displayed excellent photocatalytic performance with an apparent quantum yield of 45.6% at 365 nm [15]. However, given that the scalable application of photocatalytic water splitting, low-cost and earth-abundant cocatalysts are critically welcomed [26–28]. Two-dimensional layer transition metal dichalcogenides–known as MX_2 where M and X

are transition metal and chalcogen, respectively–have attracted increasing attention in the field of photocatalytic water splitting due to their fascinating intrinsic features [29–32]. For example, MoS_2-tipped CdS nanorods were prepared for hydrogen generation by Du and co-workers [33]. Interestingly, our previous work suggested that WSe_2 nanosheets were an efficient cocatalyst for photocatalytic hydrogen generation and accelerated charge separation are expected in WSe_2-semiconductor photosystems [34,35]. Reddy et al. loaded layer-dependent WSe_2 nanosheets on CdS nanorods and the designed CdS/WSe_2 heterojunction displayed enhanced photocatalytic hydrogen generation [36]. In addition, WSe_2-PANI nanohybrids were achieved via a sonication-assisted solution method, and they showed stable and photosensitive hydrogen evolution [37]. Compared with other transition metal dichalcogenides, WSe_2 nanosheets owned superior electrical conductivity and abundant active sites [38,39]. In addition, WSe_2 semiconductors displayed excellent photostability as well [40]. All these made it a promising cocatalysts for hydrogen evolution. However, WSe_2 decorated TiO_2 photocatalysts have been rarely reported for water splitting so far and they might exhibit exciting photocatalytic performance if they were coupled together. In addition, many approaches have been applied to construct cocatalysts–semiconductor photosystems and the mechanical grinding method is regarded as the simplest and scalable way to achieve efficient and stable heterojunctions, which is favorable for practical application of photocatalytic water splitting [41–44].

Inspired by these findings, in this work, we applied a facile mechanical grinding method to decorate TiO_2 nanoparticles with WSe_2 nanosheets. Transmission electron microscope, X-ray diffraction, X-ray photoelectron spectrometer, UV-Vis, Photoluminescence, and time-resolved Photoluminescence were applied to study the morphology, crystal structure, composition, and optical properties of the prepared nanocomposites. It was discovered that as-prepared WSe_2/TiO_2 heterojunctions displayed boosted photocatalytic activity and a highest hydrogen generation rate of 2.28 mmol/g·h, which was 114 times higher than pristine TiO_2 and was achieved with an apparent quantum yield of 43.8% at 365 nm. The improved photocatalytic performance was attributed to the efficient charge separation and abundant active sites. This work paves the way for exploitation of TiO_2-based catalysts for photocatalytic water splitting.

2. Results and Discussions

The synthesize procedure was schematically illustrated in Figure S1. WSe_2 nanosheets were prepared via a hot injection method and then they was mixed with TiO_2 nanoparticles. The powders were mechanically ground for 30 min and the micro-structures of as-prepared products were studied using TEM and HR-TEM. The obtained TiO_2 catalysts displayed heterogeneous nanoparticles as Figure 1a shows. The lattice spacing of 0.35 nm, which was attributed to the (101) plane of TiO_2, was recorded in HR-TEM images. The prepared WSe_2 displayed nanosheet morphology (about ~20 nm) with only a few layers, and a lattice spacing of 0.24 nm was characterized. After mechanical grinding, WSe_2 nanosheets could be characterized on the surface of TiO_2 nanoparticles. In addition, the corresponding lattice spacing of 0.35 nm (TiO_2) and 0.65 nm (WSe_2) could be clearly observed as Figure 1f shows. Furthermore, STEM and EDX elemental mappings were carried out to obtain the spatial distribution of WSe_2 and TiO_2 in the prepared nanocomposites. It was discovered that WSe_2 nanosheets were homogeneously distributed over the area of TiO_2 nanoparticles with some aggregations. Thus, we can conclude that WSe_2/TiO_2 heterostructures with an intimate contact were successfully obtained by the facile mechanical grinding method.

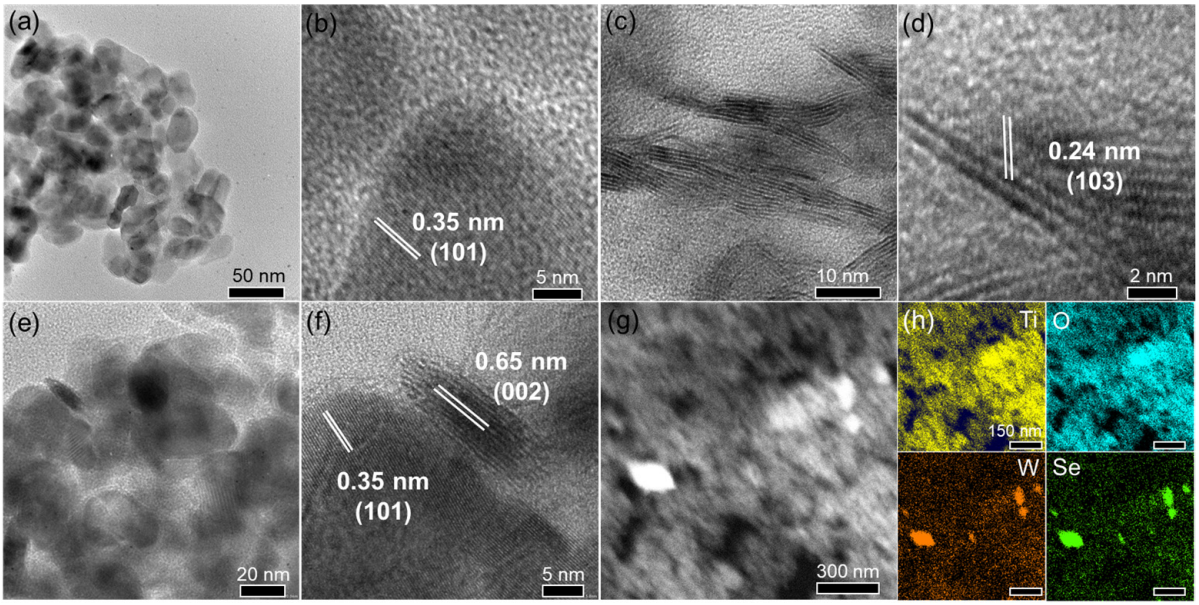

Figure 1. (**a**–**f**) TEM and HR-TEM images of TiO_2 nanoparticles (**a**,**b**), WSe_2 nanosheets (**c**,**d**), and TW-2 catalysts (**e**,**f**). (**g**) STEM and (**h**) corresponding EDX elemental mapping images of TW-2 catalyst.

The crystal structure and components of prepared samples were investigated by X-ray diffraction patterns. As Figure 2 shows, the typical diffraction peaks observed at 25.31°, 37.95°, 48.08°, 53.86°, 55.02°, 62.74°, 68.79°, 70.34°, and 74.93° were corresponding to the (101), (004), (200), (105), (211), (204), (116), (220), and (215) planes of anatase TiO_2 (JCPDS No.: 01-071-1166). The prepared WSe_2 nanosheets displayed broad and low diffraction peaks centered at about 13.6°, 32.1°, 37.8°, 47.20°, and 56.60°, which were attributed to the (002), (101), (103), (105), and (008) planes of hexagonal WSe_2 (JCPDS No.: 00-038-1388). In the case of the designed TW-x heterojunctions, both the diffraction peaks of TiO_2 and WSe_2 could be characterized with no clear shift, indicating that the mechanical grinding method did not alter the crystal structure of TiO_2 and WSe_2. Therefore, it can be concluded that the prepared samples were composed of TiO_2 and Wse_2 semiconductors.

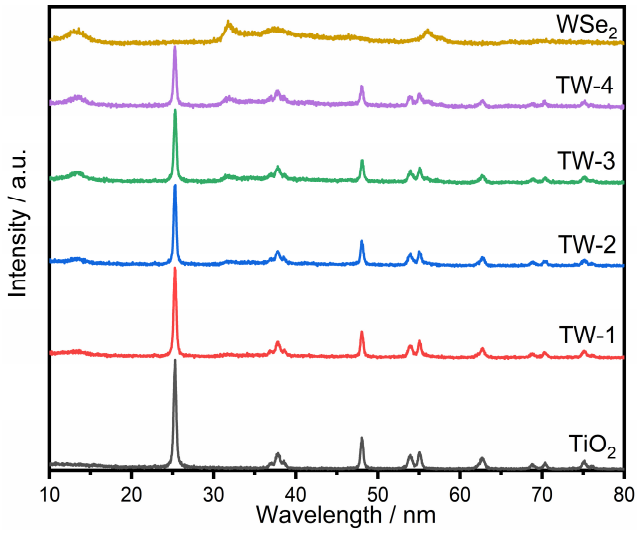

Figure 2. XRD patterns of pure TiO_2, WSe_2, and TW-x samples.

In order to investigate the surface chemical composition and valence states of prepared catalysts, XPS studies were conducted, and the spectra are shown in Figure 3. Doublet

peaks centered at 458.33 eV (Ti $2p_{3/2}$) and 464.03 eV (Ti $2p_{1/2}$) were observed, suggesting a predominant chemical state of Ti^{4+} in TiO_2 [12,45,46]. The O 1s spectrum contained two peaks centered at 529.56 eV and 531.41 eV. The former one was attributed to the lattice oxygen in TiO_2, while the latter was assigned to surface hydroxyl (O–H) groups [47–49]. Furthermore, the W 4f spectrum could be deconvoluted into four peaks appearing at 31.52 eV, 33.62 eV, 35.32 eV, and 37.50 eV. The former doublet peaks were ascribed to the +4 chemical state of the W element, which was in accordance with previous reports [50,51]. The latter two small peaks were attributed to the +6 chemical state of the W element, suggesting an oxidation of WSe_2 during the synthesis procedure [34,52]. The appearance of peak at 54.10 eV in Se 3d spectrum suggested the Se^{2-} in WSe_2 nanosheet [53,54]. Comparatively, the binding energy of Ti and O elements was slightly higher than pristine TiO_2, while the binding energy of W and Se was lower than single WSe_2 when they were coupled together. The shifted binding energies reveal the change of electron density around the atoms, and the results suggested TiO_2 was an electron donor and that WSe_2 was an electron acceptor in the prepared TW-x samples [6,55]. Moreover, it can be seen that the W^{6+} was apparently increased, indicating a strong interaction of the W–O bond in prepared TW-2 heterojunctions, which would be favorable to the interfacial charge transfer from TiO_2 to WSe_2.

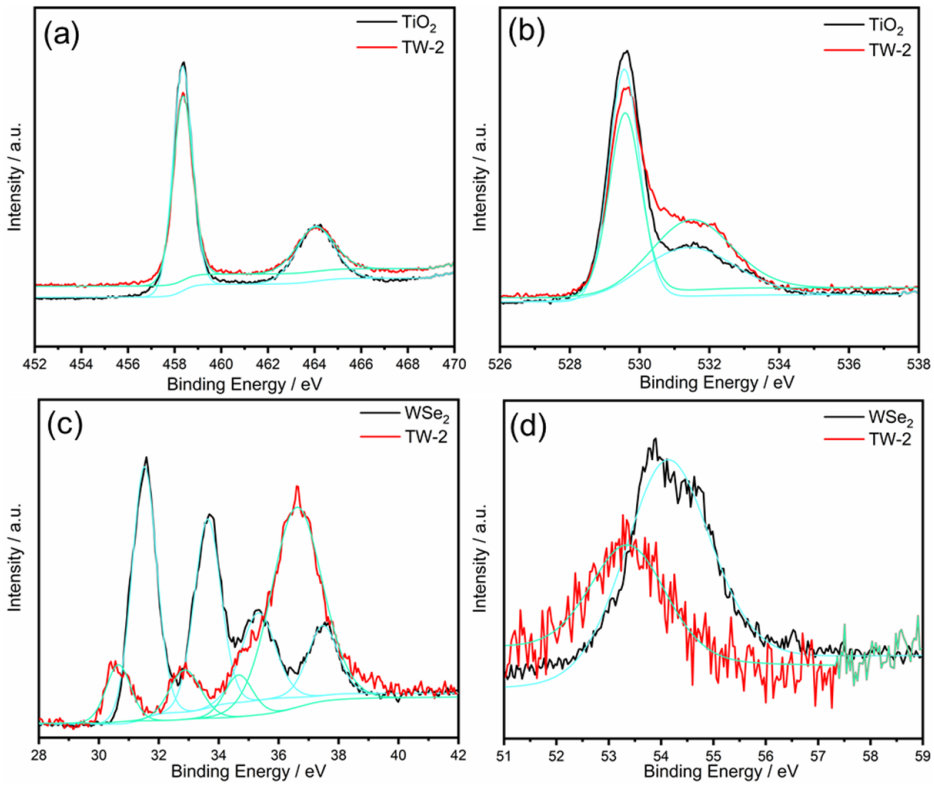

Figure 3. XPS spectra of Ti (**a**), O (**b**), W (**c**), and Se (**d**) for pure TiO_2, WSe_2, and TW-2 samples.

The light absorption properties of TiO_2, WSe_2 nanosheets, and TW-x samples were recorded by UV-Vis absorption spectra. It was discovered that the absorption edge of TiO_2 was centered at about 390 nm with weak absorption in the visible light region as Figure 4 shows. The bandgap of TiO_2 was determined to be 3.21 eV using the Kubelka–Munk method (Figure S4), which is similar to previous reports [15,24]. A strong light absorption spectrum in the entire visible region with two broad bands at about ~528 nm and ~730 nm was recorded for the prepared WSe_2 nanosheets (Figure S3), indicating the 2H phase of WSe_2 [39,40]. The absorption edge of the prepared TW-x catalysts exhibited a slightly red shift and gradually enhanced light absorbance in the visible region, which was ascribed to the light absorption of WSe_2 cocatalysts in TW-x. As expected, the

enhanced light absorption properties would benefit the photocatalytic performance of WSe_2/TiO_2 heterojunctions.

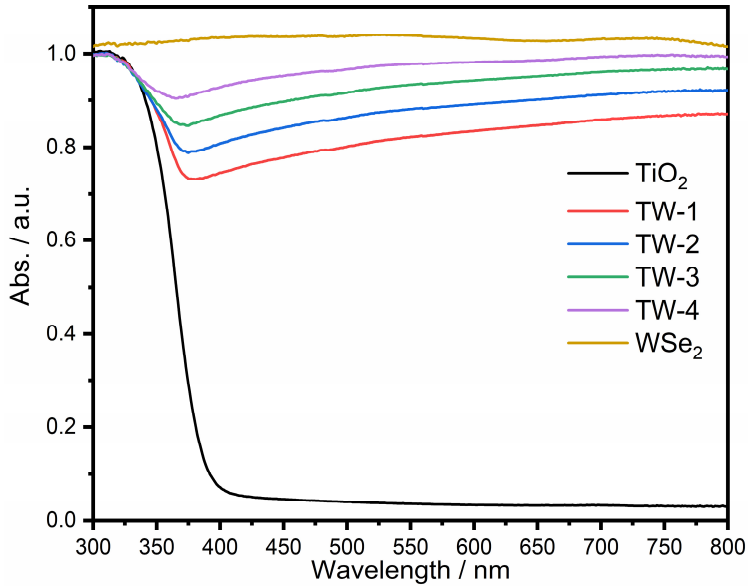

Figure 4. UV-Vis absorption spectra of TiO_2, WSe_2, and TW-x samples.

To unveil the photo-induced charge carriers transfer and recombination, photoluminescence spectra were analyzed. Commonly, the intensity of PL emission represents the utilization of photo-induced electron holes, and a strong emission band means severe charge carrier recombination [56,57]. As Figure 5a shows, steady-state PL emission of TiO_2 nanoparticles exhibited a broad and strong band centered at about ~450 nm under the excitation of 375 nm, which was associated with electron–hole recombination near the band-edges of TiO_2 [15,58]. The PL emission was obviously quenched while WSe_2/TiO_2 heterostructures were constructed via the mechanical grinding method, indicating that the recombination of photo-induced charges was largely inhibited [58–60]. In order to reveal the charge separation in depth, time-resolved PL spectra was carried out and a biexponential function fitting was applied to analyze the decay kinetics. The average lifetime of TiO_2 was calculated to be 1.48 ns according to the following Equation (1). Comparatively, the average lifetime was shorter for TW-2 (1.27 ns) than that of TiO_2 alone. The fast decay indicated that photo-induced electrons could quickly transfer from TiO_2 to WSe_2 for water reduction according to the above analysis.

$$t_A = \frac{A_1\tau_1^2 + A_2\tau_2^2}{A_1\tau_1 + A_2\tau_2} \quad (1)$$

Mott–Schottky analysis was applied to determine the flat band potentials of TiO_2 and WSe_2 nanosheets. It was known that the flat band potential was approximated to the conduction band position for n type semiconductors while the flat band potential was approximated to valence band position for p type semiconductors [9,36]. As Figure 6 shows, the Mott–Schottky curves of TiO_2 and WSe_2 exhibited positive slopes, which suggested an n-type semiconductor for the obtained TiO_2 and WSe_2. The conduction band positions were determined to be −0.131 and −0.016 V vs. NHE for TiO_2 and WSe_2 according to the flat band potentials based on Mott–Schottky curves. The higher conduction band position of TiO_2 than WSe_2 indicated that photo-induced electrons could transfer from TiO_2 to WSe_2 nanosheets for water reduction during the photocatalytic reaction.

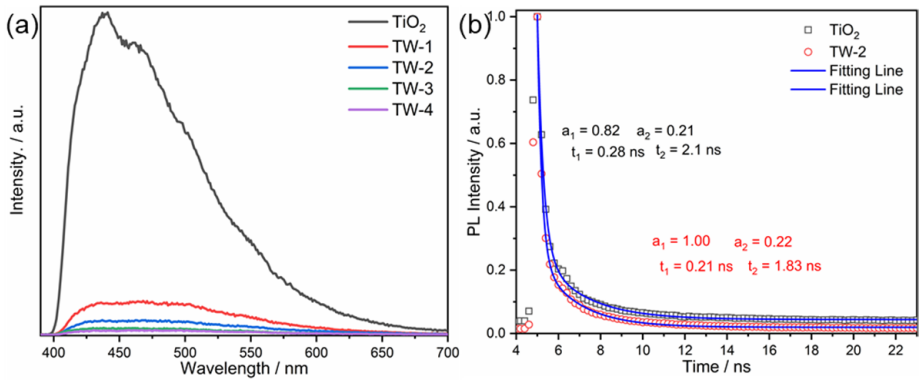

Figure 5. (**a**) Steady-state PL spectra of TiO_2, WSe_2, and TW-x samples and (**b**) PL emission decay spectra of TiO_2 and TW-2.

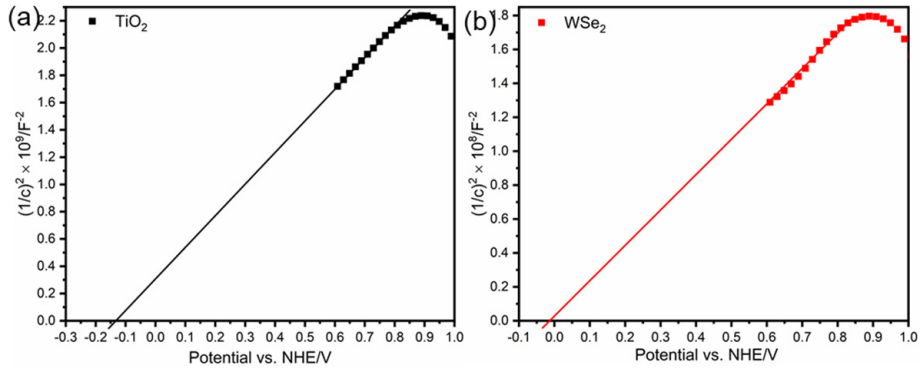

Figure 6. Mott-Schottky plots of TiO_2 (**a**) and WSe_2 (**b**).

The photocatalytic performance of the as-obtained samples was assessed by adding 10 mg of catalysts into 30 mL of an aqueous solution containing 6 mL of methanol as the hole scavenger. As Figure 7 shown, the pristine TiO_2 displayed a low hydrogen evolution activity with a rate of 0.02 mmol/g·h. No hydrogen evolution could be detected for WSe_2 nanosheets because of the strong binding energies of photo-induced excitons [61]. Notably, TW-x nanocomposites, with a coupled WSe_2 nanosheet with TiO_2 nanoparticle, all exhibited the evidently boosted photocatalytic hydrogen generation activity. The remarkable promotion effect of TW-x for photocatalytic performance should benefit from the efficient charge transfer from TiO_2 to WSe_2 and the abundant active site provide by WSe_2. However, the excessive amount of WSe_2 nanosheets led to a decreased hydrogen evolution rate. On one hand, the photoactive sites of TiO_2 might be blocked by the agglomerated WSe_2. On the other hand, the excessive amount of WSe_2 would encroach on the light absorption of TiO_2 nanoparticles and reduce the photoexcitation of TiO_2 because the bare WSe_2 shows no hydrogen evolution activity [35]. Consequently, the optimized TW-2 catalysts showed the highest hydrogen evolution rate of 2.28 mmol/g·h, 114 times higher than that of TiO_2 alone. The corresponding apparent quantum yield was estimated to be 43.8% at 365 nm, which was substantially greater than that of most reported cocatalysts-TiO_2 photocatalysts. Furthermore, the photocatalytic stability was also investigated, and no significant decrease was observed during the four cycles tests. The superior photocatalytic performance and excellent stability made WSe_2/TiO_2 nanocomposites a promising material for photocatalytic water splitting.

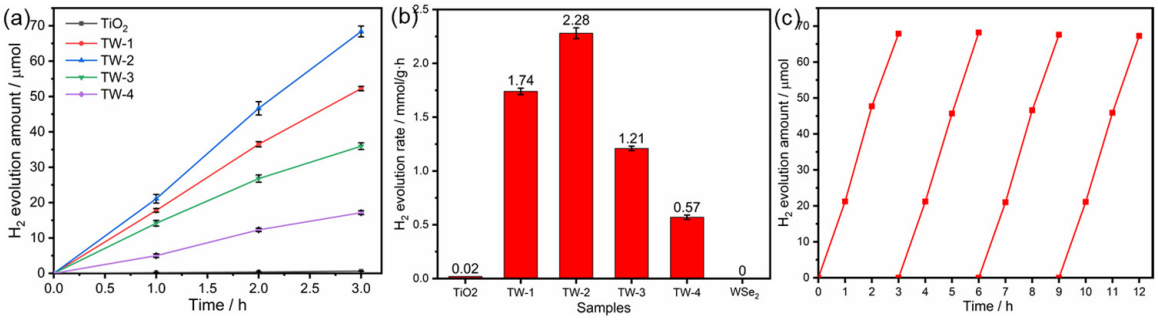

Figure 7. (**a**) Time-dependent H_2 evolution amount, (**b**) average H_2 evolution rates of TiO_2 and TW-x samples, and (**c**) cyclic hydrogen evolution activity of TW-2. A total of 10 mg of prepared photocatalysts was added into 30 mL of water containing 6 mL of methanol as sacrificial agent.

Based on the above results, the photocatalytic mechanism of the prepared TW-x heterostructures was proposed and schematically elucidated in Figure 8 and Equations (2)–(6). Under simulated solar light irradiation, both the TiO_2 and WSe_2 were excited. WSe_2 nanosheets served as electron acceptors to extract photo-induced electrons from TiO_2 and then reduced water to hydrogen. The holes on TiO_2 would be consumed by the added methanol. Moreover, the strong interaction and intimate contact between TiO_2 and WSe_2 was favorable for accelerating the interfacial charge transfer and separation [49,62]. As a result, the photocatalytic efficiency was greatly enhanced compared with TiO_2 alone. It is well known that the morphology of TiO_2, phase of WSe_2 nanosheets, and contact manners between TiO_2 and WSe_2 would have an important effect on the photocatalytic efficiency of WSe_2/TiO_2 heterojunctions. This will be investigated in the future.

$$TiO_2 + h\nu \rightarrow TiO_2(e) + TiO_2(h) \quad (2)$$

$$WSe_2 + h\nu \rightarrow WSe_2(e) + WSe_2(h) \quad (3)$$

$$TiO_2(e) + TiO_2(h) + WSe_2 \rightarrow TiO_2 + TiO_2(h) + WSe_2(e) \quad (4)$$

$$2H^+ + WSe_2(e) \rightarrow WSe_2 + H_2 \quad (5)$$

$$TiO_2(h) + WSe_2(h) + CH_3OH \rightarrow TiO_2 + WSe_2 + CO_2 + H_2O \quad (6)$$

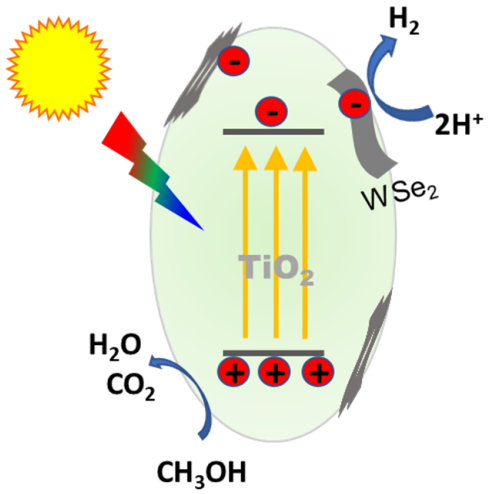

Figure 8. Schematic diagram of the photocatalytic water splitting over TW-x catalysts.

3. Materials and Methods

3.1. Chemicals

All chemicals were used as received without further purification. $W(CO)_6$, Ph_2Se_2 (diphenyl diselenide), and TOPO (trioctylphosphine oxide) were obtained from Sigma-Aldrich (St. Louis, MO, USA). Hexane, methanol, and ethanol were purchased from Sinopharm Chemical Reagent Co., Ltd (Shanghai, China). TiO_2 was purchased from Nanjing XFNANO Materials Tech Co. LTD. The water used in the synthesis and reaction was deionized with a resistivity of 18.2 MΩ·cm.

3.2. Sample Preparation

WSe_2 semiconductors. WSe_2 semiconductors were synthesized via a hot-injection method according to our previous reports with slight modifications [34]. Specifically, 48 mmol of TOPO and 0.5 mmol of $W(CO)_6$ were added into a 100 mL three-neck flask. The flask was degassed at 120 °C for 1 h. Then, it was heated to 330 °C under N_2 flow to dissolve the chemicals. At this point, 2 mmol of TOPO and 1 mmol of Ph_2Se_2 were added into a vial and heated to dissolve the chemicals completely by using a dryer. The Se-TOPO solution was rapidly injected into the reaction solution, and the flask was kept at 330 °C for 1 h. After cooling to room temperature, the precipitates were centrifuged with hexane and ethanol 5 times, and WSe_2 nanosheets were obtained by drying in vacuum at 60 °C for 8 h.

WSe_2/TiO_2 catalysts. The WSe_2/TiO_2 catalysts were prepared via a facial mechanical grinding method. Namely, a certain amount of the prepared WSe_2 and obtained TiO_2 was mixed and ground gently for 30 min at room temperature, and then the powder was collected. The weight ratio of WSe_2 and (WSe_2 + TiO_2) was adjusted to be 1:10, 2:10, 3:10, and 4:10, and the samples were labeled TW-1, TW-2, TW-3, and TW-4, respectively.

3.3. Sample Characterization

The morphology of the prepared samples was characterized on a field-emission transmission electron microscope (FE-TEM, JEOL JEM 2100 microscope, 300 kV) equipped with energy dispersing X-ray spectroscopy (EDX). The acceleration voltage was 300 kV. The crystal structure of the studied samples was characterized using a Rigaku Smartlab-9 kW X-ray diffractometer with Cu Kα radiation working at 40 kV/40 mA. X-ray photoelectron spectroscopy spectra (XPS) were collected using Escalab Xi+ X-ray photoelectron spectroscopy (Thermo Fisher Scientific, Waltham, MA, USA), and the binding energies were calibrated using adventitious carbon (C 1s peak, 284.8 eV) as a reference. The light absorption features of the materials were recorded on a Perkin-Elmer Lambda 950 spectrophotometer with $BaSO_4$ as reference. Steady state and time-resolved photoluminescence spectra at room temperature were recorded on a PicoQuant FT-300 and FT-100 fluorescence spectrophotometer under 375 nm irradiation. Mott–Schottky analysis was carried out on a CHI 760E electrochemical workstation using a standard three-electrode cell. The reference electrode and the counter electrode were Ag/AgCl (saturated KCl solution) and Pt plate. A total of 1 mg of the samples was dispersed in a mixed solution containing 250 μL of water, 250 μL of ethanol, and 10 μL of Nafion solution. It was ultrasonicated for 30 min, and 3.5 μL of the suspension was coated on the glassy carbon rotating disk electrode. After being dried at room temperature for 12 h, the prepared electrode was used as working electrode. N_2-saturated Na_2SO_4 solution (0.5 M, pH = 6.8) was used as the electrolyte.

3.4. Photocatalytic Hydrogen Generation

The photocatalytic hydrogen evolution reaction was conducted using a homemade side-irradiation Pyrex glass reactor. The temperature for the photocatalytic reaction was maintained at 35 °C by thermostatic circulating water. The side irradiation area was about 7.06 cm^2. A PLS-SXE 300+/UV Xe lamp (Perfect Light) was employed as light source (the spectrum was shown in Figure S5) and it worked at 12 mA. A total of 10 mg of the as-prepared photocatalysts was added into 30 mL of deionized water containing 6 mL of methanol as the sacrificial reagent. The solution was constantly stirred and sonicated for

15 min and then bubbled with N_2 to eliminate the air completely before light irradiation. The amount of hydrogen evolution was measured by a gas chromatograph (Bruker GC-450, Nax Zeolite column, TCD detector, and N_2 carrier). Apparent quantum yield (AQY) was defined by the following equation using a 365 nm band-pass filter, in which N_H was the number of evolved H_2 molecules and N_P was the number of incident photons [8,42].

$$\mathrm{AQY}(\%) = \frac{2N_H}{N_P} \times 100\% \quad (7)$$

4. Conclusions

To summarize, we demonstrated that mechanical grinding is a facile way to construct WSe_2/TiO_2 nanocomposites and that loading of WSe_2 can not only inhibit electron–hole recombination of TiO_2 but also provide active sites for water reduction. With the optimization of the weight ratio of $WSe_2/(WSe_2 + TiO_2)$, the prepared photocatalysts displayed the highest hydrogen evolution rate of 2.28 mmol/g·h, which corresponds to an apparent quantum yield of 43.8% at 420 nm. These findings shed light on rational design and construction of noble-metal-free cocatalysts decorated TiO_2 semiconductors for water splitting.

Supplementary Materials: The following supporting information can be downloaded at: https://www.mdpi.com/article/10.3390/catal12121668/s1, Figure S1: Scheme illustration of synthesis procedure of TW-x catalysts; Figure S2: TEM image of WSe_2 nanosheets with low magnification; Figure S3: UV-Vis absorption spectra of WSe_2 nanosheets from 300 nm to 1000 nm; Figure S4: Band-gap evaluation of TiO_2 from Tauc plot; Figure S5: The spectrum of Xe lamp used for light irradiation; Table S1: Fitting data for photoluminescence emission decay curves using a biexponential function; Table S2: Binding energies of studied samples; Table S3: Comparison of hydrogen evolution for cocatalysts-TiO_2 photocatalysts. References: [63–68].

Author Contributions: Conceptualization, X.G.; methodology, X.G., X.L. and J.S.; validation, X.G., G.Z. and S.L.; formal analysis, X.G.; investigation, X.G. and X.L.; resources, X.G.; data curation, X.G. and G.Z.; writing—original draft preparation, X.G.; writing—review and editing, X.G., X.L., J.S., G.Z. and S.L.; supervision, X.G. and S.L.; project administration, X.G.; funding acquisition, X.G. All authors have read and agreed to the published version of the manuscript.

Funding: This research was funded by the National Natural Science Foundation of China (No. 52106259), the China Postdoctoral Science Foundation (2021M692005), and the China Fundamental Research Funds for the Central Universities (GK202103110).

Institutional Review Board Statement: Not applicable.

Informed Consent Statement: Not applicable.

Data Availability Statement: The data used to support the study are included in the article.

Conflicts of Interest: The authors declare no conflict of interest.

References

1. Chen, S.; Takata, T.; Domen, K. Particulate photocatalysts for overall water splitting. *Nat. Rev. Mater.* **2017**, *2*, 17050. [CrossRef]
2. Khan, M.M.; Rahman, A. Chalcogenides and chalcogenide-based heterostructures as photocatalysts for water splitting. *Catalysts* **2022**, *12*, 1338. [CrossRef]
3. Serra, J.M.; Borrás-Morell, J.F.; García-Baños, B.; Balaguer, M.; Plaza-González, P.; Santos-Blasco, J.; Catalán-Martínez, D.; Navarrete, L.; Catalá-Civera, J.M. Hydrogen production via microwave-induced water splitting at low temperature. *Nat. Energy* **2020**, *5*, 910–919. [CrossRef]
4. Zhao, D.; Wang, Y.; Dong, C.-L.; Huang, Y.-C.; Chen, J.; Xue, F.; Shen, S.; Guo, L. Boron-doped nitrogen-deficient carbon nitride-based z-scheme heterostructures for photocatalytic overall water splitting. *Nat. Energy* **2021**, *6*, 388–397. [CrossRef]
5. Ming, M.; Yuan, H.; Yang, S.; Wei, Z.; Lei, Q.; Lei, J.; Han, Z. Efficient red-light-driven hydrogen evolution with an anthraquinone organic dye. *J. Am. Chem. Soc.* **2022**, *144*, 19680–19684. [CrossRef]
6. Guo, X.; Liu, X.; Yan, J.; Liu, S. Heteroepitaxial growth of core-shell ZnO/CdS heterostructure for efficient and stable photocatalytic hydrogen generation. *Int. J. Hydrog. Energy* **2022**, *47*, 34410–34420. [CrossRef]
7. Willkomm, J.; Orchard, K.L.; Reynal, A.; Pastor, E.; Durrant, J.R.; Reisner, E. Dye-sensitized semiconductors modified with molecular catalysts for light-driven H_2 production. *Chem. Soc. Rev.* **2016**, *45*, 9–23. [CrossRef]

8. Zhang, Y.; Zong, S.; Cheng, C.; Shi, J.; Guo, P.; Guan, X.; Luo, B.; Shen, S.; Guo, L. Rapid high-temperature treatment on graphitic carbon nitride for excellent photocatalytic H_2-evolution performance. *Appl. Catal. B Environ.* **2018**, *233*, 80–87. [CrossRef]
9. Wang, M.; Xu, S.; Zhou, Z.; Dong, C.; Guo, X.; Chen, J.; Huang, Y.; Shen, S.; Chen, Y.; Guo, L.; et al. Atomically dispersed janus nickel sites on red phosphorus for photocatalytic overall water splitting. *Angew. Chem. Int. Ed. Engl.* **2022**, *61*, e202204711.
10. Guo, X.; Liu, X.; Yan, J.; Liu, S. Heterointerface engineering of ZnO/CdS heterostructures via ZnS layer for photocatalytic water splitting. *Chem. A Eur. J.* **2022**, *144*, e202202662.
11. Guo, Q.; Ma, Z.; Zhou, C.; Ren, Z.; Yang, X. Single molecule photocatalysis on TiO_2 surfaces. *Chem. Rev.* **2019**, *119*, 11020–11041. [CrossRef] [PubMed]
12. Wei, T.; Zhu, Y.-N.; An, X.; Liu, L.; Cao, X.; Liu, H.; Qu, J. Defect modulation of Z-scheme TiO_2/Cu_2O photocatalysts for durable water splitting. *ACS Catal.* **2019**, *9*, 8346–8354. [CrossRef]
13. Thanh Thuy, C.T.; Shin, G.; Jieun, L.; Kim, H.D.; Koyyada, G.; Kim, J.H. Self-doped carbon dots decorated TiO_2 nanorods: A novel synthesis route for enhanced photoelectrochemical water splitting. *Catalysts* **2022**, *12*, 1281. [CrossRef]
14. Fujishima, A.; Honda, K. Electrochemical photolysis of water at a semiconductor electrode. *Nature* **1972**, *238*, 37–38. [CrossRef]
15. Ruan, X.; Cui, X.; Cui, Y.; Fan, X.; Li, Z.; Ba, K.; Jia, G.; Zhang, H.; Zhang, H. Favorable energy band alignment of TiO_2 anatase/rutile heterophase homojunctions yields photocatalytic hydrogen evolution with quantum efficiency exceeding 45.6%. *Adv. Energy Mater.* **2022**, *12*, 2200298. [CrossRef]
16. Cheng, Q.; Yuan, Y.-J.; Tang, R.; Liu, Q.-Y.; Bao, L.; Wang, P.; Zhong, J.; Zhao, Z.; Yu, Z.-T.; Zou, Z. Rapid hydroxyl radical generation on (001)-facet-exposed ultrathin anatase TiO_2 nanosheets for enhanced photocatalytic lignocellulose-to-H_2 conversion. *ACS Catal.* **2022**, *12*, 2118–2125. [CrossRef]
17. Shimura, K.; Yoshida, H. Heterogeneous photocatalytic hydrogen production from water and biomass derivatives. *Energy Environ. Sci.* **2011**, *4*, 2467. [CrossRef]
18. AlSalka, Y.; Al-Madanat, O.; Curti, M.; Hakki, A.; Bahnemann, D.W. Photocatalytic H_2 evolution from oxalic acid: Effect of cocatalysts and carbon dioxide radical anion on the surface charge transfer mechanisms. *ACS Appl. Energy Mater.* **2020**, *3*, 6678–6691. [CrossRef]
19. Hakki, A.; AlSalka, Y.; Mendive, C.B.; Ubogui, J.; dos Santos Claro, P.C.; Bahnemann, D. Hydrogen production by heterogeneous photocatalysis. In *Encyclopedia of Interfacial Chemistry: Surface Science and Electrochemistry*; Elsevier: Amsterdam, The Netherlands, 2018; pp. 413–419.
20. Wang, Y.; Liu, X.; Zheng, C.; Li, Y.; Jia, S.; Li, Z.; Zhao, Y. Tailoring TiO_2 nanotube-interlaced graphite carbon nitride nanosheets for improving visible-light-driven photocatalytic performance. *Adv. Sci.* **2018**, *5*, 1700844. [CrossRef]
21. Shi, L.; Liu, H.; Ning, S.; Ye, J. Localized surface plasmon resonance effect enhanced Cu/TiO_2 core–shell catalyst for boosting CO_2 hydrogenation reaction. *Catal. Sci. Technol.* **2022**, *12*, 6155–6162. [CrossRef]
22. Chen, X.; Liu, L.; Yu, P.Y.; Mao, S.S. Increasing solar absorption for photocatalysis with black hydrogenated titanium dioxide nanocrystals. *Science* **2011**, *331*, 746–750. [CrossRef] [PubMed]
23. Wei, T.; Ding, P.; Wang, T.; Liu, L.-M.; An, X.; Yu, X. Facet-regulating local coordination of dual-atom cocatalyzed TiO_2 for photocatalytic water splitting. *ACS Catal.* **2021**, *11*, 14669–14676. [CrossRef]
24. Chen, Y.; Soler, L.; Armengol-Profitós, M.; Xie, C.; Crespo, D.; Llorca, J. Enhanced photoproduction of hydrogen on Pd/TiO_2 prepared by mechanochemistry. *Appl. Catal. B Environ.* **2022**, *309*, 121275. [CrossRef]
25. Sordello, F.; Pellegrino, F.; Prozzi, M.; Minero, C.; Maurino, V. Controlled periodic illumination enhances hydrogen production by over 50% on Pt/TiO_2. *ACS Catal.* **2021**, *11*, 6484–6488. [CrossRef]
26. Moon, H.S.; Hsiao, K.C.; Wu, M.C.; Yun, Y.; Hsu, Y.J.; Yong, K. Spatial separation of cocatalysts on Z-scheme organic/inorganic heterostructure hollow spheres for enhanced photocatalytic H_2 evolution and in-depth analysis of the charge-transfer mechanism. *Adv. Mater.* **2022**, *34*, e2200172. [CrossRef]
27. Liu, J.; Bao, Y.; Liu, Y.; Yang, J.; Fujita, T.; Zeng, D. Fast one-pot synthesis of a Se-rich MnCdSe solid solution for highly efficient cocatalyst-free photocatalytic H_2 evolution. *Chem. Commun.* **2022**, *58*, 6425–6428. [CrossRef]
28. Cai, M.; Cao, S.; Zhou, Z.; Wang, X.; Shi, K.; Cheng, Q.; Xue, Z.; Du, X.; Shen, C.; Liu, X.; et al. Fabrication of Ni_2P cocatalyzed CdS nanorods with a well-defined heterointerface for enhanced photocatalytic H_2 evolution. *Catalysts* **2022**, *12*, 417. [CrossRef]
29. Peng, W.; Li, Y.; Zhang, F.; Zhang, G.; Fan, X. Roles of two-dimensional transition metal dichalcogenides as cocatalysts in photocatalytic hydrogen evolution and environmental remediation. *Ind. Eng. Chem. Res.* **2017**, *56*, 4611–4626. [CrossRef]
30. Eftekhari, A. Tungsten dichalcogenides (WS_2, WSe_2, and WTe_2): Materials chemistry and applications. *J. Mater. Chem. A* **2017**, *5*, 18299–18325. [CrossRef]
31. Chen, J.; Wu, X.J.; Lu, Q.; Zhao, M.; Yin, P.F.; Ma, Q.; Nam, G.H.; Li, B.; Chen, B.; Zhang, H. Preparation of CdS_ySe_{1-y}-MoS_2 heterostructures via cation exchange of pre-epitaxially synthesized $Cu_{2-x}S_y$-Se_{1-y}-MoS_2 for photocatalytic hydrogen evolution. *Small* **2021**, *17*, e2006135. [CrossRef]
32. Jun, S.E.; Hong, S.; Choi, S.; Kim, C.; Ji, S.G.; Lee, S.A.; Yang, J.E.; Lee, T.H.; Sohn, W.; Kim, J.Y.; et al. Boosting unassisted alkaline solar water splitting using silicon photocathode with TiO_2 nanorods decorated by edge-rich MoS_2 nanoplates. *Small* **2021**, *17*, e2103457. [CrossRef] [PubMed]
33. Du, M.; Zhang, Y.; Kang, S.; Guo, X.; Ma, Y.; Xing, M.; Zhu, Y.; Chai, Y.; Qiu, B. Trash to treasure: Photo reforming of plastic waste into commodity chemicals and hydrogen over MoS_2-tipped CdS nanorods. *ACS Catal.* **2022**, *12*, 12823–12832. [CrossRef]

34. Guo, X.; Guo, P.; Wang, C.; Chen, Y.; Guo, L. Few-layer WSe_2 nanosheets as an efficient cocatalyst for improved photocatalytic hydrogen evolution over $Zn_{0.1}Cd_{0.9}S$ nanorods. *Chem. Eng. J.* **2020**, *383*, 123183. [CrossRef]
35. Guo, X.; Li, Q.; Liu, Y.; Jin, T.; Chen, Y.; Guo, L.; Lian, T. Enhanced light-driven charge separation and H_2 generation efficiency in WSe_2 nanosheet-semiconductor nanocrystal heterostructures. *ACS Appl. Mater. Interfaces* **2020**, *12*, 44769–44776. [CrossRef] [PubMed]
36. Arun Joshi Reddy, K.; Amaranatha Reddy, D.; Hye Hong, D.; Gopannagari, M.; Putta Rangappa, A.; Praveen Kumar, D.; Kyu Kim, T. Impact of the number of surface-attached tungsten diselenide layers on cadmium sulfide nanorods on the charge transfer and photocatalytic hydrogen evolution rate. *J. Colloid. Interface Sci.* **2022**, *608*, 903–911. [CrossRef] [PubMed]
37. Kannichankandy, D.; Pataniya, P.M.; Sumesh, C.K.; Solanki, G.K.; Pathak, V.M. WSe_2-PANI nanohybrid structure as efficient electrocatalyst for photo-enhanced hydrogen evolution reaction. *J. Alloys Compd.* **2021**, *876*, 160179. [CrossRef]
38. Wang, X.; Lu, Q.; Sun, Y.; Liu, K.; Cui, J.; Lu, C.; Dai, H. Fabrication of novel p-n-p heterojunctions ternary $WSe_2/In_2S_3/ZnIn_2S_4$ to Enhance visible-light photocatalytic activity. *J. Environ. Chem. Eng.* **2022**, *10*, 108354. [CrossRef]
39. Wang, W.; Li, Y.; Li, M.; Shen, H.; Zhang, W.; Zhang, J.; Liu, T.; Kong, X.; Bi, H. Metallic phase WSe_2 nanoscrolls for the hydrogen evolution reaction. *New J. Chem.* **2022**, *46*, 8381–8384. [CrossRef]
40. Qorbani, M.; Sabbah, A.; Lay, Y.; Kholimatussadiah, S.; Quadir, S.; Huang, C.; Shown, I.; Huang, Y.; Hayashi, M.; Chen, K.; et al. Atomistic insights into highly active reconstructed edges of monolayer 2H-WSe_2 photocatalyst. *Nat. Commun.* **2022**, *13*, 1256. [CrossRef]
41. Saruyama, M.; Pelicano, C.M.; Teranishi, T. Bridging electrocatalyst and cocatalyst studies for solar hydrogen production via water splitting. *Chem. Sci.* **2022**, *13*, 2824–2840. [CrossRef]
42. Pelicano, C.M.; Saruyama, M.; Takahata, R.; Sato, R.; Kitahama, Y.; Matsuzaki, H.; Yamada, T.; Hisatomi, T.; Domen, K.; Teranishi, T. Bimetallic synergy in ultrafine cocatalyst alloy nanoparticles for efficient photocatalytic water splitting. *Adv. Funct. Mater.* **2022**, *32*, 2202987. [CrossRef]
43. Cantarella, M.; Gorrasi, G.; Mauro, A.; Scuderi, M.; Nicotra, G.; Fiorenza, R.; Scire, S.; Scalisi, M.; Crundo, M.; Privitera, V.; et al. Mechanical milling: A sustainable route to induce structural transformations in MoS_2 for applications in the treatment of contaminated water. *Sci. Rep.* **2019**, *9*, 974. [CrossRef] [PubMed]
44. Ansari, S.A.; Cho, M.H. Simple and large-scale construction of MoS_2-g-C_3N_4 heterostructures using mechanochemistry for high performance electrochemical supercapacitor and visible light photocatalytic applications. *Sci. Rep.* **2017**, *7*, 43055. [CrossRef] [PubMed]
45. Wang, X.; Jiang, S.; Huo, X.; Xia, R.; Muhire, E.; Gao, M. Facile preparation of a TiO_2 quantum dot/graphitic carbon nitride heterojunction with highly efficient photocatalytic activity. *Nanotechnology* **2018**, *29*, 205702. [CrossRef] [PubMed]
46. Guan, X.; Zong, S.; Tian, L.; Zhang, Y.; Shi, J. Construction of $SrTiO_3$-$LaCrO_3$ solid solutions with consecutive band structures for photocatalytic H_2 evolution under visible light irradiation. *Catalysts* **2022**, *12*, 1123. [CrossRef]
47. Tian, M.; Ma, M.; Xu, B.; Chen, C.; He, C.; Hao, Z.; Albilali, R. Catalytic removal of 1,2-dichloroethane over $LaSrMnCoO_6$/H-ZSM-5 composite: Insights into synergistic effect and pollutant-destruction mechanism. *Catal. Sci. Technol.* **2018**, *8*, 4503–4514. [CrossRef]
48. Tian, M.; Guo, X.; Dong, R.; Guo, Z.; Shi, J.; Yu, Y.; Cheng, M.; Albilali, R.; He, C. Insight into the boosted catalytic performance and chlorine resistance of nanosphere-like meso-macroporous $CrO_x/MnCo_3O_x$ for 1,2-dichloroethane destruction. *Appl. Catal. B Environ.* **2019**, *259*, 118018. [CrossRef]
49. Guo, X.; Chen, Y.B.; Qin, Z.X.; Su, J.Z.; Guo, L.J. Facet-selective growth of cadmium sulfide nanorods on zinc oxide microrods: Intergrowth effect for improved photocatalytic performance. *ChemCatChem* **2018**, *10*, 153–158. [CrossRef]
50. Biswas, M.; Ali, A.; Cho, K.Y.; Oh, W.C. Novel synthesis of WSe_2-graphene-TiO_2 ternary nanocomposite via ultrasonic technics for high photocatalytic reduction of CO_2 into CH_3OH. *Ultrason. Sonochem.* **2018**, *42*, 738–746. [CrossRef]
51. Park, Y.J.; So, H.S.; Hwang, H.; Jeong, D.S.; Lee, H.J.; Lim, J.; Kim, C.G.; Shin, H.S. Synthesis of 1T WSe_2 on an oxygen-containing substrate using a single precursor. *ACS Nano* **2022**, *16*, 11059–11065. [CrossRef]
52. Smyth, C.M.; Addou, R.; McDonnell, S.; Hinkle, C.L.; Wallace, R.M. WSe_2-contact metal interface chemistry and band alignment under high vacuum and ultra high vacuum deposition conditions. *2D Mater.* **2017**, *4*, 025084. [CrossRef]
53. Xia, M.; Ning, J.; Wang, D.; Feng, X.; Wang, B.; Guo, H.; Zhang, J.; Hao, Y. Ammonia-assisted synthesis of gypsophila-like 1T-WSe_2/graphene with enhanced potassium storage for all-solid-state supercapacitor. *Chem. Eng. J.* **2021**, *405*, 126611. [CrossRef]
54. Kadam, S.R.; Enyashin, A.N.; Houben, L.; Bar-Ziv, R.; Bar-Sadan, M. Ni-WSe_2 nanostructures as efficient catalysts for electrochemical hydrogen evolution reaction (HER) in acidic and alkaline media. *J. Mater. Chem. A* **2020**, *8*, 1403–1416. [CrossRef]
55. Zhang, K.; Fujitsuka, M.; Du, Y.; Majima, T. 2D/2D heterostructured CdS/WS_2 with efficient charge separation improving H_2 evolution under visible light irradiation. *ACS Appl. Mater. Interfaces* **2018**, *10*, 20458–20466. [CrossRef] [PubMed]
56. Liu, L.; Du, S.; Guo, X.; Xiao, Y.; Yin, Z.; Yang, N.; Bao, Y.; Zhu, X.; Jin, S.; Feng, Z. Water-stable nickel metal-organic framework nanobelts for cocatalyst-free photocatalytic water splitting to produce hydrogen. *J. Am. Chem. Soc.* **2022**, *144*, 2747–2754. [CrossRef] [PubMed]
57. Bhatt, H.; Goswami, T.; Yadav, D.K.; Ghorai, N.; Shukla, A.; Kaur, G.; Kaur, A.; Ghosh, H.N. Ultrafast hot electron transfer and trap-state mediated charge carrier separation toward enhanced photocatalytic activity in g-$C_3N_4/ZnIn_2S_4$ heterostructure. *J. Phys. Chem. Lett.* **2021**, *12*, 11865–11872. [CrossRef]
58. Feng, K.; Sun, T.; Hu, X.; Fan, J.; Yang, D.; Liu, E. 0D/2D $Co_{0.85}Se/TiS_2$ p–n heterojunction for enhanced photocatalytic H_2 Evolution. *Catal. Sci. Technol.* **2022**, *12*, 4893–4902. [CrossRef]
59. Li, D.; Zhao, Y.; Miao, Y.; Zhou, C.; Zhang, L.P.; Wu, L.Z.; Zhang, T. Accelerating electron-transfer dynamics by TiO_2 immobilized reversible single-atom copper for enhanced artificial photosynthesis of urea. *Adv. Mater.* **2022**, e2207793. [CrossRef]

60. Zhao, H.; Li, C.; Liu, L.; Palma, B.; Hu, Z.; Renneckar, S.; Larter, S.; Li, Y.; Kibria, M.G.; Hu, J.; et al. n-p heterojunction of TiO_2-NiO core-shell structure for efficient hydrogen generation and lignin photoreforming. *J. Colloid. Interface Sci.* **2021**, *585*, 694–704. [CrossRef]
61. Zhao, C.; Tao, W.; Chen, Z.; Zhou, H.; Zhang, C.; Lin, J.; Zhu, H. Ultrafast electron transfer with long-lived charge separation and spin polarization in WSe_2/C_{60} heterojunction. *J. Phys. Chem. Lett.* **2021**, *12*, 3691–3697. [CrossRef]
62. Guo, X.; Chen, Y.; Qin, Z.; Wang, M.; Guo, L. One-step hydrothermal synthesis of $Zn_xCd_{1-X}S$/ZnO heterostructures for efficient photocatalytic hydrogen production. *Int. J. Hydrog. Energy* **2016**, *41*, 15208–15217. [CrossRef]
63. Zhong, W.; Gao, D.; Yu, H.; Fan, J.; Yu, J. Novel amorphous nicus H_2-evolution cocatalyst: Optimizing surface hydrogen desorption for efficient photocatalytic activity. *Chem. Eng. J.* **2021**, *419*, 129652. [CrossRef]
64. Xu, L.; Li, L.; Ao, Y.; Long, F.; Guan, J. Engineering highly efficient photocatalysts for hydrogen production by simply regulating the solubility of insoluble compound cocatalysts. *Int. J. Hydrogen Energy* **2014**, *39*, 11486–11493. [CrossRef]
65. Xiao, S.; Liu, P.; Zhu, W.; Li, G.; Zhang, D.; Li, H. Copper nanowires: A substitute for noble metals to enhance photocatalytic H_2 generation. *Nano Lett* **2015**, *15*, 4853–4858. [CrossRef]
66. Du, F.; Lu, H.; Lu, S.; Wang, J.; Xiao, Y.; Xue, W.; Cao, S. Photodeposition of amorphous MoS_X cocatalyst on TiO_2 nanosheets with {001} facets exposed for highly efficient photocatalytic hydrogen evolution. *Int. J. Hydrogen Energy* **2018**, *43*, 3223–3234. [CrossRef]
67. Wang, P.; Xu, S.; Chen, F.; Yu, H. Ni nanoparticles as electron-transfer mediators and NiS_x as interfacial active sites for coordinative enhancement of H_2-evolution performance of TiO_2. *Chinese J. Catal.* **2019**, *40*, 343–351. [CrossRef]
68. Xiang, Q.; Yu, J.; Jaroniec, M. Synergetic effect of MoS_2 and graphene as cocatalysts for enhanced photocatalytic H_2 production activity of TiO_2 nanoparticles. *J. Am. Chem. Soc.* **2012**, *134*, 6575–6578. [CrossRef]